nature physics

ARTICLES

PUBLISHED ONLINE: 8 MAY 2017 | DOI: 10.1038/NPHYS4107

Quasiparticle interference and strong electron–mode coupling in the quasi-one-dimensional bands of Sr_2RuO_4

Zhenyu Wang[1†], Daniel Walkup[2,3†], Philip Derry[4], Thomas Scaffidi[5], Melinda Rak[1], Sean Vig[1], Anshul Kogar[1], Ilija Zeljkovic[2], Ali Husain[1], Luiz H. Santos[6], Yuxuan Wang[6], Andrea Damascelli[7,8], Yoshiteru Maeno[9], Peter Abbamonte[1], Eduardo Fradkin[6] and Vidya Madhavan[1*]

The single-layered ruthenate Sr_2RuO_4 is presented as a potential spin-triplet superconductor with an order parameter that may break time-reversal invariance and host half-quantized vortices with Majorana zero modes. Although the actual nature of the superconducting state is still a matter of controversy, it is believed to condense from a metallic state that is well described by a conventional Fermi liquid. In this work we use a combination of Fourier transform scanning tunnelling spectroscopy (FT-STS) and momentum-resolved electron energy loss spectroscopy (M-EELS) to probe interaction effects in the normal state of Sr_2RuO_4. Our high-resolution FT-STS data show signatures of the β-band with a distinctly quasi-one-dimensional (1D) character. The band dispersion reveals surprisingly strong interaction effects that dramatically renormalize the Fermi velocity, suggesting that the normal state of Sr_2RuO_4 is that of a 'correlated metal' where correlations are strengthened by the quasi-1D nature of the bands. In addition, kinks at energies of approximately 10 meV, 38 meV and 70 meV are observed. By comparing STM and M-EELS data we show that the two higher energy features arise from coupling with collective modes. The strong correlation effects and the kinks in the quasi-1D bands could provide important information for understanding the superconducting state.

The electronic properties of complex oxides are highly sensitive to electron–electron interactions as well as interactions of electrons with other collective modes[1–4]. Identifying these many-body effects is critical to understanding the driving forces behind many of their exotic phases. The unconventional *p*-wave superconductor Sr_2RuO_4, in particular, is a fundamentally interesting material system[5–7]. To understand its unique superconducting state with spin-triplet pairing, it is important to have an intimate knowledge of its normal state properties[8]. Yet, the effects of interactions in the normal state are yet to be sorted out, with the conventional belief that it is a Fermi liquid conflicting with reports of large band-dependent mass renormalizations and strong correlation effects[8–12]. Much of this uncertainty can be traced to the multiband nature of this system, the interplay between spin and lattice degrees of freedom[13], as well as the strong k-dependent spin–orbital entanglement of the normal state wavefunction, which makes the description of superconductivity in terms of pure spin-triplet (and/or singlet) eigenstates questionable[14].

The overall band structure of Sr_2RuO_4 is well known[8,15] and consists of three Fermi surface (FS) sheets with distinct characteristics (Fig. 1a). The three bands are primarily derived from ruthenium $4dt_{2g}$ orbitals. Hybridization between the d_{xz} and d_{yz} orbitals leads to two sets of quasi-1D FS sheets: a hole-like α sheet near X and an electron-like β sheet near Γ, while the in-plane d_{xy} orbital forms an electron-like, quasi-2D γ sheet centred at Γ. The dominant superconducting instability can be placed either on the γ band or the α and β bands in different theoretical approaches[16–20]. Consequently, the symmetry of the resulting superconducting state and the pairing 'glue' are still unclear. It is thus essential to characterize interaction effects on three bands, which may generate or assist the superconducting pairing in this material. Angle-resolved photoemission spectroscopy (ARPES) data have revealed kinks at energies of 40 meV, 50–60 meV and 70–80 meV in the dispersion of the quasi-2D γ band[4,13,21,22]. Although there have been some discussions of self-energy effects for the α band[23], no sharp features have been unambiguously identified on the quasi-1D bands[13,21,24].

In this work we study the effect of interactions on the electronic structure of Sr_2RuO_4 using the complementary techniques of FT-STS and meV-resolution M-EELS. FT-STS is a powerful tool to study electron behaviour in **r**-space and **k**-space simultaneously, and has been successfully used to study the nanoscale spectroscopic properties of high-T_C superconductors[25], heavy-fermion systems[26,27] and the bilayer strontium ruthenate[28]. M-EELS is a complementary technique for measuring the energy and dispersion of collective excitations that couple strongly to electrons[29]. So far, neither of

---

[1]Department of Physics and Frederick Seitz Materials Research Laboratory, University of Illinois Urbana-Champaign, Urbana, Illinois 61801, USA. [2]Department of Physics, Boston College, Chestnut Hill, Massachusetts 02467, USA. [3]National Institute of Standards and Technology, Gaithersburg, Maryland 20899, USA. [4]Department of Chemistry, Physical & Theoretical Chemistry, Oxford University, South Parks Road, Oxford OX1 3QZ, United Kingdom. [5]Rudolf Peierls Centre for Theoretical Physics, Oxford OX1 3NP, UK. [6]Department of Physics and Institute for condensed Matter Theory, University of Illinois at Urbana-Champaign, Urbana, Illinois 61801, USA. [7]Department of Physics & Astronomy, University of British Columbia, Vancouver, British Columbia V6T 1Z1, Canada. [8]Quantum Matter Institute, University of British Columbia, Vancouver, British Columbia V6T 1Z4, Canada. [9]Department of Physics, Graduate School of Science, Kyoto University, Kyoto 606-8502, Japan. †These authors contributed equally to this work. *e-mail: vm1@illinois.edu

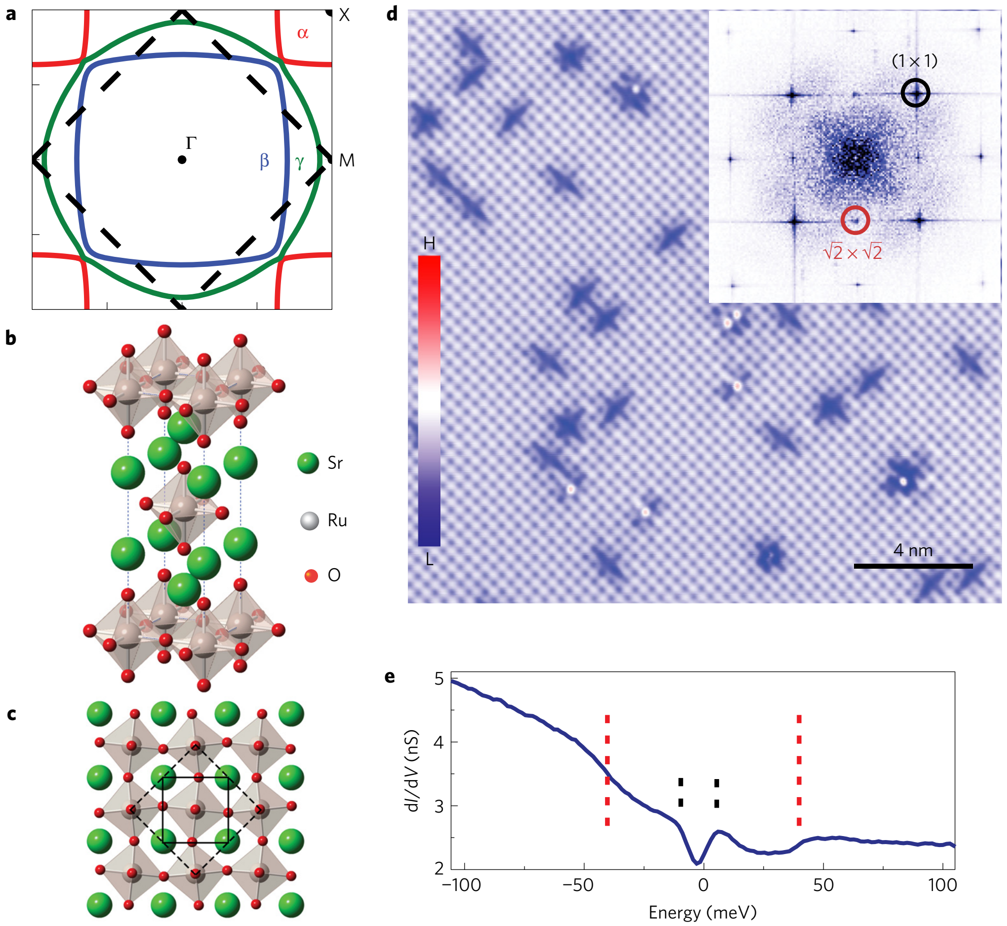

Figure 1 | Fermi surfaces and crystal structure of Sr_2RuO_4. **a**, Bulk Fermi surfaces of Sr_2RuO_4 calculated with tight binding model. Dashed lines denote the new Brillouin zone caused by $\sqrt{2}\times\sqrt{2}$ surface reconstruction. **b**, Crystal structure of Sr_2RuO_4 showing the Ru-centred octahedra. **c**, A schematic top view of the surface reconstruction with rotated RuO_6 octahedra. The unit cells with and without rotation are denoted by the dashed black square and solid black square, respectively. **d**, Topographic image of Sr_2RuO_4 showing a uniform square lattice with spacing of ∼3.9 Å between atoms (bias voltage $V_S = 70$ mV, tunnelling current $I_t = 100$ pA). The inset shows its Fourier transform: the black circle represents a Bragg peak, and the red circle the $\sqrt{2}\times\sqrt{2}$ reconstruction. **e**, Typical differential conductance spectrum taken in a defect-free region ($I_t = 265$ pA, $V_S = 110$ mV). The red and black dashed lines denote two features with energy scales approximately 38 meV and 10 meV, respectively.

these techniques has been successfully applied to Sr_2RuO_4. Here, we use FT-STS to visualize quasiparticle interference in the normal state and determine band dispersion with high precision, which allows us to determine correlation effects as well as the effects of lattice and spin excitations on the electronic structure. Our FT-STS data reveal that the β band displays distinct signatures of quasi-1D behaviour with a dispersion that reveals a dramatic suppression of Fermi velocity. We further find a low-energy suppression of the density of states, centred approximately at the Fermi energy. These combined observations suggest that quasi-1D band character of the β band accentuates correlation effects. We note that whereas there are many studies of correlation effects in pure 1D systems, the effects on quasi-1D bands are less well known. At higher energies we find kinks in the dispersion. Modes at similar energies are observed in our M-EELS data, suggesting that they originate from the coupling of quasiparticles with collective bosonic modes such as phonons. The strong correlation effects and identification of the energy scales of kinks in the quasi-1D bands may provide key information needed to obtain a microscopic model for the superconducting state. Our success in obtaining high-quality data using FT-STS for the first time provides a new pathway for exploring the quasiparticles below T_c, which would reveal the momentum dependence of the superconducting energy gap, $\Delta(k)$, and help distinguish the pairing mechanism in Sr_2RuO_4.

Sr_2RuO_4 has a layered perovskite structure similar to cuprate superconductors[5] (Fig. 1b). Cleaving could in principle expose two kinds of natural non-polar surfaces, either SrO or RuO_2 planes[18], although cleaving at the SrO plane is thought to be more likely. The topographic features can be highly dependent on the cleave temperature[15,30]. Sr_2RuO_4 single crystals studied here were cleaved at ∼80 K *in situ* and then transferred to a scanning tunnelling microscope (STM) held at 4.3 K. Figure 1d presents a typical topographic image, showing a square lattice with atomic spacing ∼3.9 Å. The 6.3 Å atomic step height seen near this scan range (Supplementary Information Part I) suggests a preferential termination layer, which we believe to be the SrO plane. The bright protrusions in the STM image are most likely Sr atoms[31] while the impurities that look like dark crosses can be tentatively assigned to CO adsorbates[32]. Although a secondary modulation is almost invisible in the topographic images, their Fourier transforms show additional peaks at $\sqrt{2}\times\sqrt{2}$ positions arising from the $(\sqrt{2}\times\sqrt{2})R45^\circ$ surface reconstruction seen in low-energy electron diffraction[31] and ARPES measurements[15]. A schematic is shown in Fig. 1c, in which RuO_6 octahedra are rotated alternately in a chequerboard pattern. The energy-integrated M-EELS data taken along the (H, H) direction in reciprocal space also shows a peak near (1/2, 1/2), corresponding to this reconstruction (Supplementary Fig. 2). At the surface, the first Brillouin zone (BZ) is reduced to half (dashed black square in Fig. 1a), which gives rise to band folding across the $(\pm\pi/a_0, 0) - (0, \pm\pi/a_0)$ lines. As we will see later, this reconstruction plays an important role in the quasiparticle interference (QPI) pattern.

A typical differential conductance spectrum is shown in Fig. 1e. This spectrum is representative of the sample: since the native impurity concentration is low, the density of states is fairly homogeneous. There are features at approximately 38 meV on both sides of the Fermi energy (E_F), which are similar to earlier data on Ti-doped Sr_2RuO_4 samples[33]. The particle–hole symmetric nature of the 38 meV peak can be clearly seen in the derivative of the spectrum (Supplementary Fig. 3) and suggests that it originates from coupling with a collective mode[34]. We also find collective modes at this energy in both the STM-derived dispersion and M-EELS data, and we will return to this energy scale later. Interestingly, similar to the spectra measured below T_c in previous work[33], our data show a low-energy gap-like feature with an energy scale of approximately 10 meV. Although the origin of this anomaly is unclear, one possibility is that it represents a suppression of the tunnelling density of states of the α and β bands due to accentuated correlation effects arising from their quasi-1D nature[35], as discussed later in this paper. Further temperature-dependent studies would be necessary to elucidate the origin of this feature.

We now apply the technique of FT-STS to Sr_2RuO_4. In FT-STS, differential conductance maps—that is, $dI/dV(\mathbf{r}, eV)$—are acquired that display spatial modulations arising from elastic scattering of quasiparticles. These maps are Fourier transformed to extract scattering vectors (Q-vectors), which connect electronic states in k-space via a set of selection rules. High-resolution FT-STS measurements can be used to measure details of the band dispersion and also reveal orbital or spin textures. Figure 2a–c show representative dI/dV $(\mathbf{r}, eV)$ maps on Sr_2RuO_4 at a few different energies. Fourier transforms of the maps display a rich array of scattering channels, as shown in Fig. 2d–l, where a sequence of inequivalent sets of scattering channels are labelled as q_i: $i = 0$, 1,2,3,4. We find that q_0 is non-dispersive. Although this feature will be discussed in further detail elsewhere, we note that it potentially originates from Friedel oscillations generated by impurities whose signatures are unusually strong due to the quasi-1D nature of the bands. Although for ease of discussion we focus on the scattering vectors along the high-symmetry directions (π, 0) and (π, π), there is of course a continuous array of scattering channels, which reflect the Fermi surface topology: these are indicated by arcs of appropriate colours in Fig. 2.

Identification of the origin of the Q-vectors requires comparison between the band structure (Fig. 3a), predicted QPI (Fig. 3c,d), and the measured data (Fig. 2 and Fig. 3b). The detailed analysis of the Q-vectors is presented in the Supplementary Information Part II, and here we only present a summary. The dominant signal in the FT is along the (π, 0) direction, labelled q_1. A complete analysis of this feature indicates that q_1 represents the intra-β-band scattering (pink arrows, also shown as pink arcs in Fig. 2). The corresponding Umklapp scattering process, labelled as q_1', is also visible in our data (dashed pink arrows). These two scattering processes are illustrated in Fig. 3a.

To understand the remaining Q-vectors we require three essential pieces of information. First, ARPES data show two β-bands, one identified as the bulk β-band and the other as a surface β-band attributed to the surface reconstruction[36,37]. In our data we also observe a second dispersing square feature labelled q_2 (orange arrows, also shown as orange arcs in Fig. 2) that emerges close to Fermi level (Fig. 2g). As discussed in detail after obtaining the dispersion, both the qualitative and quantitative behaviour of q_1 and q_2 suggest a common origin with the two ARPES β-bands. An alternative explanation for q_2 is that it originates from the α band (q_α; grey arrows in Fig. 3c and d). However, the concave shape of q_2 is identical to the curvature of q_1 (see Fig. 2i for example) and qualitatively different from the convex curvature expected of q_α (Fig. 3c,d), which indicates that this is unlikely.

Second, most of the γ band (except around $(\pi/a_0, \pi/a_0)$) is composed of the planar d_{xy} orbital. The matrix elements for the coupling of an STM tip to planar orbitals are typically small[28], so the signal from this band is mostly absent from our data. However, around $(\pi/a_0, \pi/a_0)$, an arc-shaped feature labelled q_3 appears, which can be distinguished from q_2 by a discontinuity as we trace the contours of the β band. This signal potentially originates from the small portion of the γ band along the ΓX direction that acquires d_{xz}/d_{yz} orbital character due to hybridization[14], thereby making it visible to STM measurements.

Third, the rotation of the RuO_6 octahedra creates band folding at the surface. This has a distinct effect on the QPI, as seen in the comparison of theoretical calculations of the QPI with (Fig. 3d) and without band folding (Fig. 3c). One of the effects of band folding is the appearance of parallel lines inside the yellow rectangle in Fig. 3d. These folded features are labelled q_4, and can be seen clearly in our data (Figs 3b, 2h–l and Supplementary Information Part II).

Having understood the dominant features in the Fourier transforms, we now discuss their dispersions. Linecuts of the FTs were taken along two high-symmetry directions, (π, 0) (corresponding to scattering vectors in the ΓM direction) and (π, π) (the ΓX direction). The position of each peak in the linecut was determined by fitting a Gaussian function with a linear background (Supplementary Information Part III). The peak positions representing the energy and momentum-resolved Q-vectors are plotted in Fig. 4a. This plot does not include q_4 since it represents a folded band and is not an independent Q-vector. By comparing the shapes of q_1 and q_2 in the FTs shown in Fig. 2, as well as their dispersion, it is apparent that q_2 and q_1 are related to each other, with one branch being shifted in momentum with respect to the other. In essence q_2 and q_1 behave like two versions of the β band. Although there are a few possible explanations for such a splitting, such as surface induced spin–orbit effect or magnetic fluctuations, as mentioned earlier, a secondary β band was also observed in ARPES measurements[36,37] which was attributed to a surface band. Quantitatively, the two Fermi wavevectors (k_F) observed by us are 0.62 ± 0.02 and 0.68 ± 0.02 (in unit of π/a_0). These values are identical to those observed in multiple ARPES experiments[36–38], indicating that the STM and ARPES bands have the same origin. ARPES studies identified the band with the larger k_F to be the bulk branch while the band with the smaller k_F was identified as the surface branch. Interestingly, we find support for this scenario by looking at band folding effects. We find that the band identified by ARPES to be a surface band (q_2) shows clear folding (Fig. 2h–l), as evidenced by the presence of q_4, whereas the band folding is suppressed for q_1 below the Fermi energy, as seen in Fig. 2d–g. The comparison with ARPES, as well as the differences in band folding effects for q_1 and q_2, suggest that we measure both the surface and bulk bands by STM, with q_1 being identified as the bulk band.

A striking feature of the dispersion of the β band is the change in slope of q_1 and q_2 near E_F, indicating a strong renormalization of the Fermi velocity (Fig. 4a). From our data, the Fermi velocity of q_1 is renormalized to 0.46 eV Å. Previous ARPES measurements of the Fermi velocity show a large variation for data from different groups[13,21,22,24,39], with values ranging from 0.5 eV Å to 1.5 eV Å, making a clear comparison difficult (see Supplementary Information Part III). De Haas–van Alphen oscillations (dHvA)[8] yield an average value of 0.65 eV Å which is larger than the STM measured value by a factor of 1.4. A possible explanation for this discrepancy lies in the details of what the two probes measure. Most of our QPI data arise from a narrow range of momenta where the β band is flattest, and hence most nested. Our signal is strong in this direction and the intensity fades away from these points. It is

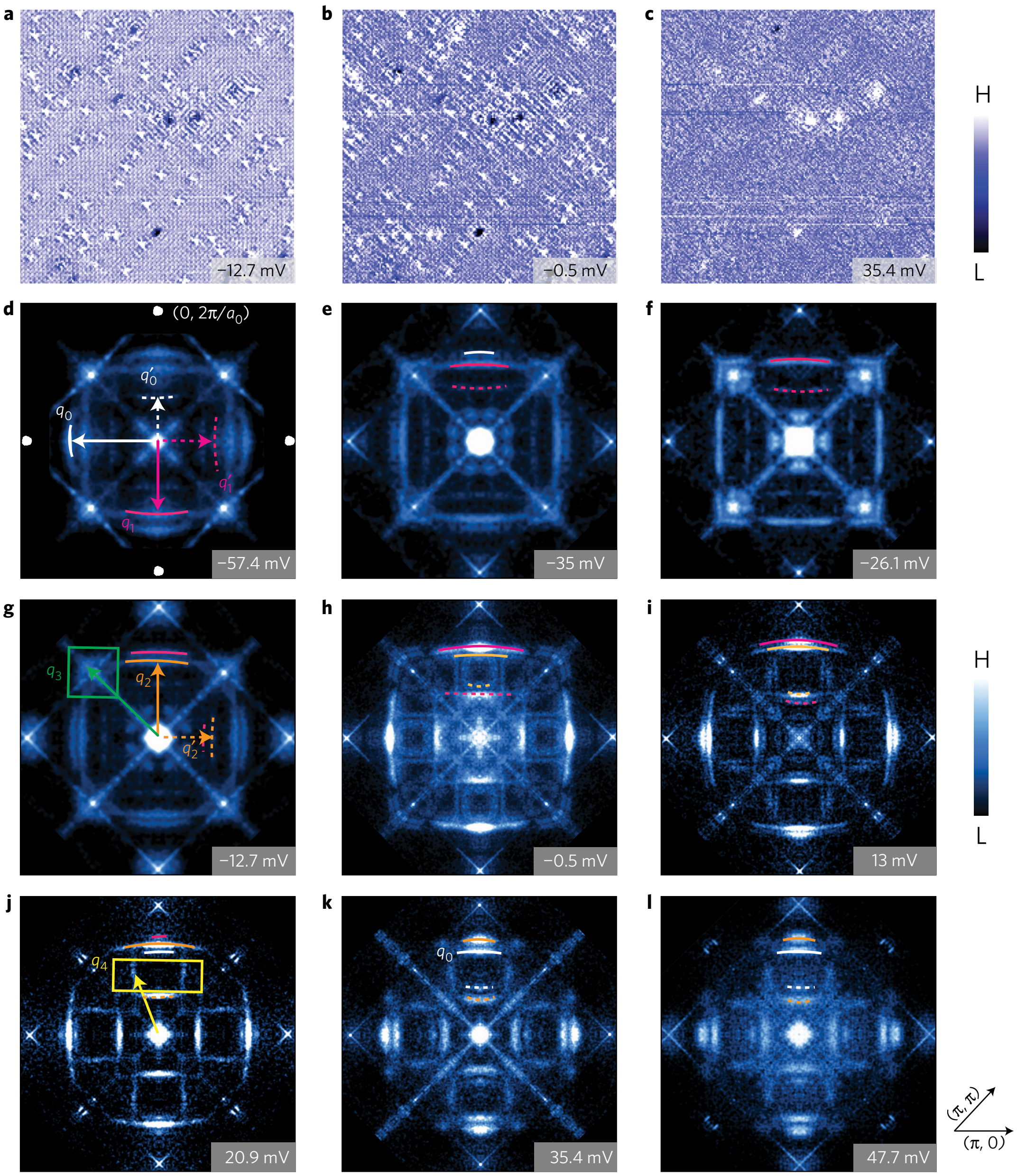

Figure 2 | Quasiparticle interference (QPI) of Sr_2RuO_4. a–c, Spatially resolved d*I*/d*V* conductance maps at −12.7 meV, −0.5 meV and 35.4 meV, respectively. For clarity, a 34-nm-square field of view (FOV) is cropped from a larger 78 nm × 78 nm FOV which we used to obtain the Fourier transform images. **d–l**, Drift-corrected and symmetrized Fourier transforms of d*I*/d*V* conductance maps. White dots in **d** indicate the Bragg peaks. The spectral weight near the centre has been reduced by removing the low-frequency signals originating from defects. Dominant scattering vectors are indicated by q_i ($i = 0$, 1, 2, 3, 4). Dashed arrows and arcs denote their Umklapp processes. H, high; L, low.

possible that the quasi-1D nature of the β band at these momenta strengthen correlation effects which can in turn increase the degree of the mass enhancement in this range of momenta. The dHvA slope on the other hand represents an average over the entire Fermi surface, thereby diluting the effects seen by us, which may account for the differences between the two measurements. In essence, our data reveal that the correlation effects on the β band are much larger than previously thought.

In fact, the quasi-1D nature of the β band may play an important role in strengthening correlation effects, as seen in many facets of our data. First, the β band contour shown in Fig. 2 is remarkably flat for much of its extension. Second, the brightness of the q_1/q_2 scattering vectors in the ΓM direction (Supplementary Fig. 8) indicate that there is a singularity in the number of scattering processes with the same magnitude in this direction. The quasi-1D nature is also reflected in the momentum-dependent nature of the renormalization suggested by comparison with dHvA in the previous paragraph. In general, quasi-1D electronic states are expected to share many key features of true 1D systems, including non-Fermi liquid behaviours such as a suppression of the one-particle density of states, a large downward renormalization of the Fermi velocity and a large enhancement of the charge and spin susceptibilities at $2k_F$ (ref. 35). In quasi-1D systems, however, these features are rounded by an eventual crossover to 2D Fermi liquid behaviour[40,41]. Many of the predicted effects of 1D bands on the electronic structure are borne out by the STM data presented here, including a zero-bias anomaly in the tunnelling DOS at an energy scale of about 10 meV and a downward renormalization of the Fermi velocity over the same energy scale. These observations taken together support the scenario of enhanced correlation effects on

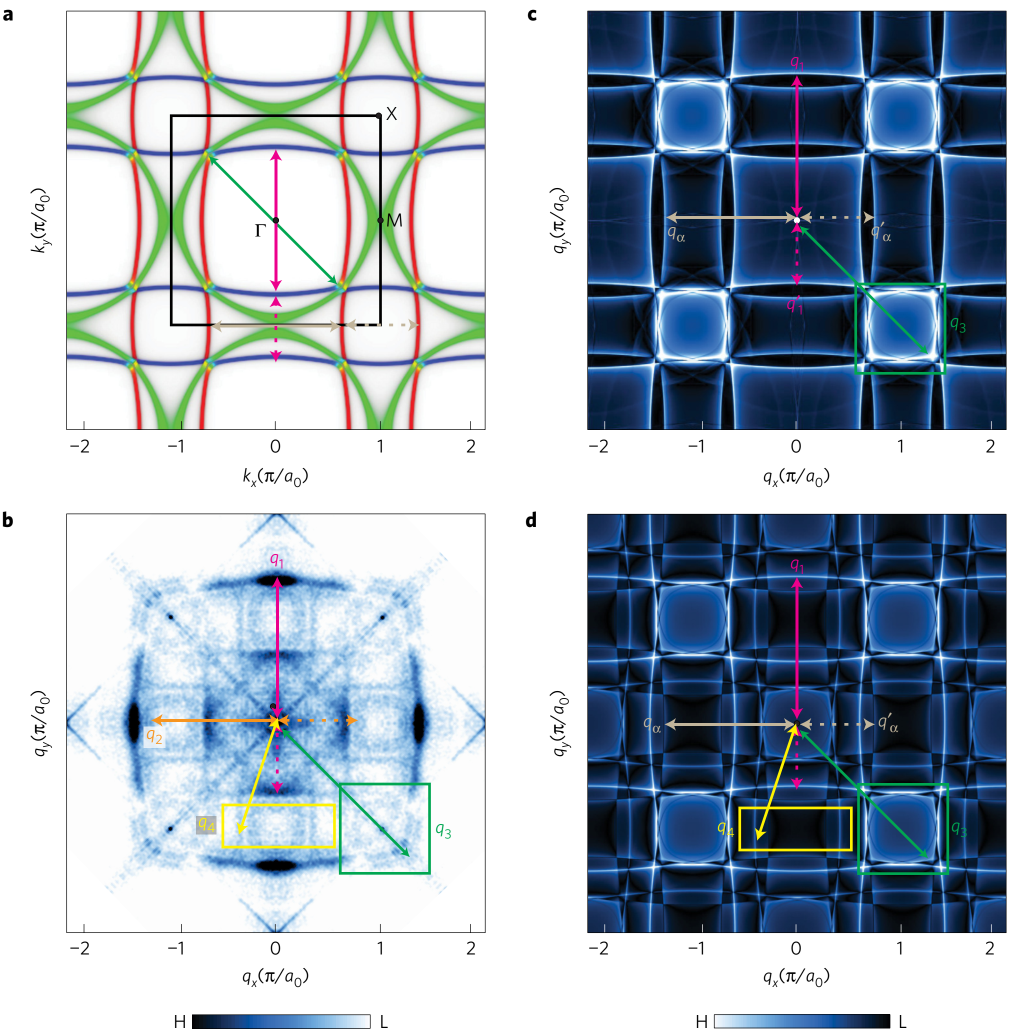

Figure 3 | Comparison of the FT-STS images with predicted QPI patterns. **a**, Spectral density at the Fermi level for the α, β and γ bulk bands. The relative contributions of each orbital to the bands are colour-coded. Red, $4d_{xz}$; blue, $4d_{yz}$; green, $4d_{xy}$. Arrows with different colours denote possible scattering channels. For a better view, the CECs are shown in the extended zone. **b**, QPI map at the Fermi energy (−0.5 meV, same as in Fig. 2h) and inequivalent Q-vectors are indicated either by arrows or coloured squares. **c**,**d**, Theoretically simulated QPI patterns using the T-matrix approach for the original unfolded FSs (**c**), and the folded bands (**d**). q_1 and q_1' represent intra-band scattering of bulk β band and its Umklapp process, respectively, while q_2 and q_2' represent the surface β band; q_3 represents a small portion of intra-γ-band scattering; q_4 represents scattering processes between unfolded bands and their folded replicas; q_α and q_α' in **c** and **d** represent intra-α-band scattering and the corresponding Umklapp processes.

the β band bolstered by its quasi-1D nature. Our observations also suggest that this system may be close to a charge and/or spin density wave instability, as implied by earlier neutron scattering data[42].

In addition to interaction effects near E_F, the dispersion in Fig. 4a reveals clear kinks at multiple energy scales. Kinks are ubiquitous in many correlated electron systems, and reflect self-energy renormalizations, which carry important information about the effective interactions. Among high-T_C superconductors, for example, kinks in the dispersion have been observed in cuprates[2,3] and Fe-based superconductors[43]. However, simply observing kinks in the dispersion is typically not sufficient to understand their origin, since both electron–electron as well as electron–boson interactions may result in kinks[1]. In the following discussion, we employ the complementary techniques of STM and M-EELS to not only identify the energy scales of the kinks, but also their potential origin. Kinks were observed in the STM data at energies of ~35 meV (ω_1) and ~70 meV (ω_2) in the dispersion of q_1, and at ~32 meV above the Fermi level for q_2. These energy scales are also clearly visible in the extracted self-energy $\mathrm{Re}\Sigma$ ($\mathbf{k}$, ω) shown in Fig. 4b obtained by subtracting a bare band from the observed dispersion. To avoid artefacts, the bare band was simply chosen to be a straight line connecting two points of $q(\omega = 0)$ and $q(\omega = \pm 110\,\mathrm{meV})$. The details of the bare band used would be important if one were trying to obtain quantitative information about the self-energy[23]. However, this treatment is sufficient for our analysis, where we concentrate on the peak positions. The peak energies of ω_1 and ω_2 in the extracted $\mathrm{Re}\Sigma$ ($\mathbf{k}$, ω) are ~37 meV and ~73 meV. To further pin down the energy scales and the potential origin of these kinks, we turn to our M-EELS measurements. The results are shown in Fig. 4c. Interestingly M-EELS data predominantly show the same two peaks, one near 38 meV (corresponding to ω_1 in the STM data) and the other at 71 meV (corresponding to ω_2). ω_1 disperses with momentum in a manner consistent with an optical phonon. However, ω_2 shows an anomalous momentum dependence, disappearing abruptly as we move away from high-symmetry points, suggestive of a surface phonon merging with a bulk band. In essence, the M-EELS data provide evidence that ω_1 and ω_2 arise from phonons that strongly couple with the quasi-1D β band in Sr_2RuO_4. We note that similar modes were observed in ARPES studies of the 2D γ band[4,13]. The similarity of these energy scales to the M-EELS data provides evidence that the ARPES kinks at

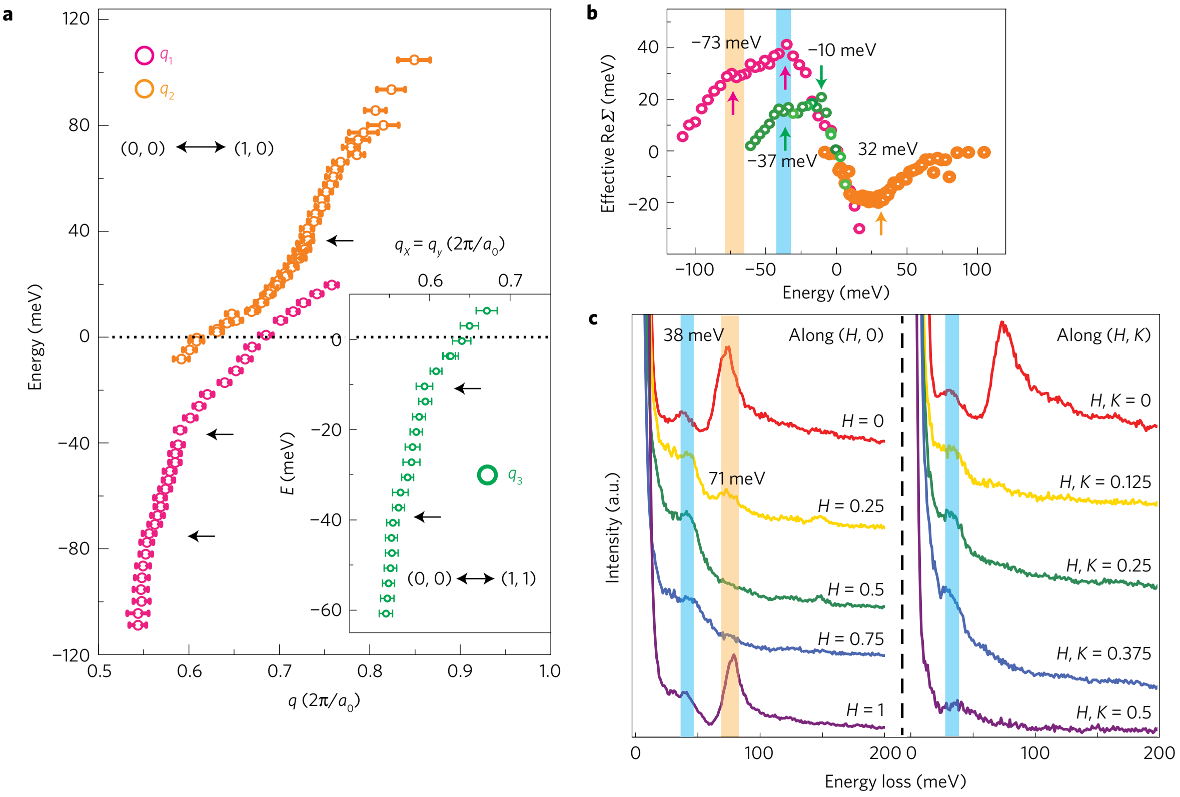

Figure 4 | Visualizing the electron-collective mode coupling in the Quasi-1D bands. a, Dispersions of the bulk β band (q_1) and surface β band (q_2) extracted by fitting peaks in linecuts along ΓM direction. These peaks reflect the dynamic nesting processes involving band structures as well as the quasiparticle self-energy. Kink features are seen at energies of about −35 meV and −70 meV for q_1, and +32 meV for q_2, as shown by arrows. (Inset) Dispersion of q_3 along the ΓX direction, which shows an additional kink at approximately −10 meV. The error bars are the sum of the standard deviation widths from the Gaussian fit, and the size of smoothing window. **b**, Corresponding effective real part of quasiparticle self-energy for the measured dispersion. A straight line connecting two points at E_F and ±110 meV (−60 meV for q_3) in the dispersion is used as the 'bare' band for each **q** dispersion. Peaks at multiple energy scales are marked with arrows: −37 and −73 meV for the bulk β band, 32 meV for the surface β band, and −10 meV and −37 meV for q_3. **c**, Momentum-resolved electron energy loss spectra taken at $T = 100$ K. Two peaks at 38 meV and 71 meV are clearly revealed, which match the energy scales of kinks seen in QPI.

these energies also arise from coupling of quasiparticles to the same phonons. Interestingly, the dispersion of q_3 along the ΓX direction (inset in Fig. 4a) shows an additional kink near 10 meV (ω_3). The background subtracted q_3 shown in Fig. 4b also clearly reveals ω_3. If one regards q_3 as the intra-γ-band scattering, ω_3 may be related to coupling with the Σ_3 phonon, which exhibits a sharp drop near the zone boundary (∼1.9 THz) and potentially enhances ferromagnetic (FM) spin fluctuations[31].

The order parameter (OP) of superconductivity and the associated gap structure in momentum space have been long-standing issues in Sr_2RuO_4. However, compelling experimental evidence favours an odd parity (triplet) state and there is evidence that the SC order spontaneously breaks time-reversal symmetry[5,6], suggesting a chiral *p*-wave state. This latter possibility has remained controversial, primarily due to the potentially different roles played by the quasi-1D and 2D bands. The most direct way to distinguish between the various predictions involving pairing on either the quasi-1D bands[17] (α, β) or the quasi-2D band[16] (γ) is to determine the momentum-dependent OP, a task not yet carried out due to the low superconducting transition temperature of ∼1 K, sub-meV magnitude of the gap and the existence of multiple bands. However, our present work gives a unique approach to directly confirm the gap structure on the 1D bands. For example, according to one theory[17], if one places the dominant superconducting gap on 1D bands, the β band would be gapped out such that the constant energy contours (CECs) of Bogoliubov quasiparticles would form around the nodes near (π, π) (ref. 18). As the result, the Bogoliubov QPI pattern, which is dominated by scattering between the ends of these banana-shaped CECs, should show clear changes compared to the normal state pattern (see Fig. 5 in ref. 18). Detailed information about $\Delta(k)$ on the β band can then be obtained by tracking the energy evolution of this pattern, which will increase our understanding of the pairing symmetry as well as provide clues on the microscopic pairing mechanism in this material. Finally, the results presented in this paper suggest that the quasi-1D character of the β band causes enhanced interaction effects, thus raising doubts on the picture that the normal state is simply a weakly correlated Fermi liquid metal. Additional experiments, including the effects of temperature and magnetic fields, will be needed to further clarify this picture.

Methods

Methods, including statements of data availability and any associated accession codes and references, are available in the online version of this paper.

Received 4 August 2016; accepted 22 March 2017;

References

1. Byczuk, K. *et al*. Kinks in the dispersion of strongly correlated electrons. *Nat. Phys.* **3,** 168–171 (2007).
2. Carbotte, J. P., Timusk, T. & Hwang, J. Bosons in high-temperature superconductors: an experimental survey. *Rep. Prog. Phys.* **74,** 066501 (2011).

3. Lanzara, A. *et al*. Evidence for ubiquitous strong electron–phonon coupling in high-temperature superconductors. *Nature* **412,** 510–514 (2001).
4. Aiura, Y. *et al*. Kink in the dispersion of layered strontium ruthenates. *Phys. Rev. Lett.* **93,** 117005 (2004).
5. Mackenzie, A. P. & Maeno, Y. The superconductivity of Sr_2RuO_4 and the physics of spin-triplet pairing. *Rev. Mod. Phys.* **75,** 657–712 (2003).
6. Kallin, C. Chiral *p*-wave order in Sr_2RuO_4. *Rep. Prog. Phys.* **75,** 042501 (2012).
7. Jang, J. *et al*. Observation of half-height magnetization steps in Sr_2RuO_4. *Science* **331,** 186–188 (2011).
8. Bergemann, C. Quasi-two-dimensional Fermi liquid properties of unconventional superconductor Sr_2RuO_4. *Adv. Phys.* **52,** 639–725 (2003).
9. Liebsch, A. & Lichtenstein, A. Photoemission quasiparticles spectra of Sr_2RuO_4. *Phys. Rev. Lett.* **84,** 1591–1594 (2000).
10. Kidd, T. E. *et al*. Orbital dependence of the Fermi liquid state in Sr_2RuO_4. *Phys. Rev. Lett.* **94,** 107003 (2005).
11. Stricker, D. *et al*. Optical response of Sr_2RuO_4 reveals universal Fermi-liquid scaling and quasiparticles beyond Laudau theory. *Phys. Rev. Lett.* **113,** 087404 (2014).
12. Zhang, G., Gorelov, E., Sarvestani, E. & Pavarini, E. Fermi surface of Sr_2RuO_4: spin-orbit and anisotropic Coulomb interaction effects. *Phys. Rev. Lett.* **116,** 106402 (2016).
13. Iwasawa, H. *et al*. Interplay among Coulomb interaction, spin–orbital interaction, and multiple electron–boson interactions in Sr_2RuO_4. *Phys. Rev. Lett.* **105,** 226406 (2010).
14. Veenstra, C. N. *et al*. Spin-orbital entanglement and the breakdown of singlets and triplets in Sr_2RuO_4 revealed by spin- and angle-resolved photoemission spectroscopy. *Phys. Rev. Lett.* **112,** 127002 (2014).
15. Damascelli, A. *et al.* Fermi surface, surface states, and surface reconstruction in Sr_2RuO_4. *Phys. Rev. Lett.* **85,** 5194–5197 (2000).
16. Rice, T. M. & Sigrist, M. Sr_2RuO_4: a electronic analogue of ^{3}He? *J. Phys. Condens. matter* **7,** L643–L648 (1995).
17. Raghu, S., Kapitulnik, A. & Kivelson, S. A. Hidden quasi-one-dimensional superconductivity in Sr_2RuO_4. *Phys. Rev. Lett.* **105,** 136401 (2010).
18. Firmo, I. A. *et al*. Evidence from tunneling spectroscopy for a quasi-one-dimensional origin of superconductivity in Sr_2RuO_4. *Phys. Rev. B* **88,** 134521 (2013).
19. Wang, Q. H. *et al*. Theory of superconductivity in a three-orbital model of Sr_2RuO_4. *Euro. Phys. Lett.* **104,** 17013 (2013).
20. Scaffidi, T., Romers, J. C. & Simon, S. H. Pairing symmetry and dominant band in Sr_2RuO_4. *Phys. Rev. B* **89,** 220510(R) (2014).
21. Iwasawa, H. *et al*. Orbital selectivity of the kink in the dispersion of Sr_2RuO_4. *Phys. Rev. B* **72,** 104514 (2005).
22. Burganov, B. *et al*. Strain control of fermiology and many-body interaction in two dimensional ruthenates. *Phys. Rev. Lett.* **116,** 197003 (2016).
23. Ingle, N. J. *et al*. Quantitative analysis of Sr_2RuO_4 angle-resolved photoemission spectra: many-body interactions in a model Fermi liquid. *Phys. Rev. B* **72,** 205114 (2005).
24. Kim, C. *et al*. Self-energy analysis of multiple-bosonic mode coupling in Sr_2RuO_4. *J. Phys. Chem. Solids* **72,** 556–558 (2011).
25. Hoffman, J. E. *et al*. Imaging quasiparticle interference in $Bi_2Sr_2CaCu_2O_{8+\delta}$. *Science* **297,** 1148–1151 (2002).
26. Allan, M. P. *et al*. Imaging Cooper pairing of heavy fermions in $CeCoIn_5$. *Nat. Phys.* **9,** 468–473 (2013).
27. Zhou, B. B. *et al*. Visualizing nodal heavy fermion superconductivity in $CeCoIn_5$. *Nat. Phys.* **9,** 474–479 (2013).
28. Lee, J. *et al*. Heavy *d*-electron quasiparticle interference and real-space electronic structures of $Sr_3Ru_2O_7$. *Nat. Phys.* **5,** 800–804 (2009).
29. Kogar, A., Vig, S., Gan, Y. & Abbamonte, P. Temperature-resolution anomalies in the reconstruction of time dynamics from energy-loss experiments. *J. Phys. B: At. Mol. Opt. Phys.* **47,** 124034 (2014).
30. Pennec, Y. *et al*. Cleaving-temperature dependence of layered-oxide surfaces. *Phys. Rev. Lett.* **101,** 216103 (2008).
31. Matzdorf, R. *et al*. Ferromagnetism stabilized by lattice distortion at the surface of the *p*-wave superconductor Sr_2RuO_4. *Science* **289,** 746–748 (2000).
32. Stöger, B. *et al*. High chemical activity of a perovskite surface: reaction of CO with $Sr_3Ru_2O_7$. *Phys. Rev. Lett.* **113,** 116101 (2014).
33. Barker, B. I. *et al*. STM studies of individual Ti impurity atoms in Sr_2RuO_4. *Physica B* **329–333,** 1334–1335 (2003).
34. Hlobil, P. *et al*. Tracing the electronic pairing glue in unconventional superconductors via inelastic scanning tunneling spectroscopy. *Phys. Rev. Lett.* **118,** 167001 (2017).
35. Fradkin, E. *Field Theories of Condensed Matter Systems* (Cambridge Univ. Press, 2013).
36. Veenstra, C. N. *et al*. Determining the surface-to-bulk progression in the normal-state electronic structure of Sr_2RuO_4 by angle-resolved photoemission and density functional theory. *Phys. Rev. Lett.* **110,** 097004 (2013).
37. Liu, S. Y. *et al*. Fermi surface sheet-dependent band splitting in Sr_2RuO_4 revealed by high-resolution angle-resolved photoemission spectroscopy. *Phys. Rev. B* **86,** 165112 (2012).
38. Zabolotnyy, V. B. *et al*. Surface and bulk electronic structure of the unconventional superconductor Sr_2RuO_4: unusual splitting of the β band. *New J. Phys.* **14,** 063039 (2012).
39. Iwasawa, H. *et al*. High-energy anomaly in the band dispersion of the ruthenate superconductor. *Phys. Rev. Lett.* **109,** 066404 (2012).
40. Carlson, E. W., Orgad, D., Kivelson, S. A. & Emery, V. J. Dimensional crossover in quasi-one-dimensional and high-T_C superconductors. *Phys. Rev. B* **62,** 3422–3437 (2000).
41. Biermann, S., Georges, A., Lichtenstein, A. & Giamarchi, T. Deconfinement transition and Luttinger to Fermi liquid crossover in quasi-one-dimensional systems. *Phys. Rev. Lett.* **87,** 276405 (2001).
42. Sidis, Y. *et al*. Evidence for incommensurate spin fluctuations in Sr_2RuO_4. *Phys. Rev. Lett.* **83,** 3320–3323 (1999).
43. Allan, M. P. *et al*. Identifying the 'fingerprint' of antiferromagnetic spin fluctuations in iron pnictide superconductors. *Nat. Phys.* **11,** 177–182 (2015).

Acknowledgements

We thank Z. Wang, H. Lin, J.C. Davis and S. Kivelson for useful conversations. STM work was supported by US Department of Energy, Scanned Probe Division under Award Number DE-SC0014335. The work was supported in part by the Gordon and Betty Moore Foundation's EPiQS Initiative through Grant GBMF4860. Y.M. acknowledges the support from the JSPS KAKENHI Grant No. JP15H05852. Theoretical work was supported in part by the Gordon and Betty Moore Foundation's EPiQS Initiative through Grant No. GBMF4305 at the Institute for Condensed Matter Theory of the University of Illinois (L.H.S. and Y.W.), and by a grant of the National Science Foundation No. DMR1408713 at the University of Illinois (E.F.). M-EELS experiments were supported by the Center for Emergent Superconductivity, DOE #DE-AC02-98CH10886. P.A. acknowledges support from Gordon and Betty Moore Foundation's EPiQS Initiative through Grant GBMF4542. T.S. acknowledges the financial support of the Clarendon Fund Scholarship, the Merton College Domus and Prize Scholarships, and the University of Oxford.

Author contributions

Z.W. and D.W. contributed equally to this work. Z.W., D.W. and V.M. designed the STM experiments, analysed the data and wrote the paper. STM experiments were performed by D.W., Z.W. and I.Z. Y.M. was responsible for single-crystal growth and structural analysis. A.D. helped with conceiving the experiment, data analysis and comparison with ARPES. E.F., L.H.S. and Y.W. conceived the theoretical explanation for this work. P.D., and T.S. performed analytical model calculations. M.R., S.V., A.K., A.H. and P.A. were involved in the M-EELS studies.

Additional information

Supplementary information is available in the online version of the paper. Reprints and permissions information is available online at www.nature.com/reprints. Publisher's note: Springer Nature remains neutral with regard to jurisdictional claims in published maps and institutional affiliations. Correspondence and requests for materials should be addressed to V.M.

Competing financial interests

The authors declare no competing financial interests.

Methods

STM measurements. High-quality Sr_2RuO_4 single crystals were grown at Kyoto University and the University of British Columbia. The samples were cleaved *in situ* at liquid nitrogen temperature (∼80 K) and then transferred into the STM head immediately. The topographies were taken in the constant current mode and all the dI/dV measurements were collected using a standard lock-in technique with 5 meV peak-to-peak modulation at a frequency of 987.5 Hz. All the STM measurements are carried out at 4.3 K using electrochemically etched tungsten tips. To obtain high-quality STM images, it is critical to have clean and sharp tips. The Lawler–Fujita drift-correction algorithm is used for the FT-QPI data to remove the drift effects[44]. The detailed FT-STS data analysis procedure is displayed in Supplementary Information Part II and more electronic dispersion results obtained on different samples and different tips are shown in Supplementary Information Part III.

M-EELS measurements. M-EELS measures the bosonic density response function, $\chi''(q, \omega)$, of a material surface[29]. These experiments were carried out at a beam energy of 50 eV on crystals of Sr_2RuO_4 cleaved under vacuum and subsequently cooled to 100 K. Elastic scattering from the (1, 0) and (1, 1) Bragg reflections was used *in situ* to construct an orientation matrix translating between diffractometer angles and reciprocal space. The Miller indices (H, K) designate the transferred momentum in tetragonal units, such that $\mathbf{q} = 2\pi(H, K)/a$, where $a = \sim 3.9$ Å is the in-plane lattice parameter.

Data availability. The data that support the plots within this paper and other findings of this study are available from the corresponding author upon reasonable request.

References

44. Lawler, M. J. *et al*. Intra-unit-cell electronic nematicity of the high-T_C copper-oxide pseudogap states. *Nature* **466,** 347–351 (2010).